Multistable inflatable origami structures at the metre scale

https://doi.org/10.1038/s41586-021-03407-4

Received: 24 August 2020

Accepted: 1 March 2021

Published online: 21 April 2021



Check for updates

David Melancon^{1,7}, Benjamin Gorissen^{1,7}, Carlos J. García-Mora^{1,2}, Chuck Hoberman^{3,4,5}

& Katia Bertoldi^{1,3,6™}

From stadium covers to solar sails, we rely on deployability for the design of large-scale structures that can quickly compress to a fraction of their size $^{1-4}$. Historically, two main strategies have been used to design deployable systems. The first and most frequently used approach involves mechanisms comprising interconnected bar elements, which can synchronously expand and retract⁵⁻⁷, occasionally locking in place through bistable elements^{8,9}. The second strategy makes use of inflatable membranes that morph into target shapes by means of a single pressure input^{10–12}. Neither strategy, however, can be readily used to provide an enclosed domain that is able to lock in place after deployment; the integration of a protective covering in linkage-based constructions is challenging and pneumatic systems require a constant applied pressure to keep their expanded shape 13-15. Here we draw inspiration from origami—the Japanese art of paper folding—to design rigid-walled deployable structures that are multistable and inflatable. Guided by geometric analyses and experiments, we create a library of bistable origami shapes that can be deployed through a single fluidic pressure input. We then combine these units to build functional structures at the metre scale, such as arches and emergency shelters, providing a direct route for building large-scale inflatable systems that lock in place after deployment and offer a robust enclosure through their stiff faces.

Large, deployable structures should ideally (1) occupy the minimum possible volume when folded, (2) be autonomous when deploying, (3) lock in place after deployment, and (4) provide a structurally robust shell (if they are designed to define a closed environment). To satisfy all these requirements, here we present an approach with roots in the Japanese art of paper folding: origami. Extensively used in robotics¹⁶⁻²⁰, metamaterials²¹⁻²⁵ and structures²⁶⁻³⁰, origami principles have the potential to lead to efficient large-scale deployable structures as they offer (1) a versatile crease-based approach to shape design³¹⁻³³, (2) an easy actuation through inflation, if enclosed ^{34–36}, (3) self-locking capabilities when designed to support multiple energy wells³⁷⁻⁴⁴, and (4) the possibility to create a protective environment through their faces. While previous origami systems have explored inflatability and multistability separately³⁴⁻⁴⁴, here we show that these two properties can co-exist, unlocking an unprecedented design space of metre-scale inflatable structures that harness multistability to maintain their deployed shape without the need for continuous actuation (see schematics in Fig. 1a).

Triangular facets as a platform for bistable and inflatable structures

To create inflatable and bistable origami structures, we start by considering a triangular building block ABC and denote with α and β the internal angles enclosed by the edges AB-AC and AB-BC, respectively (Fig. 1b). The triangle initially lies in the x-y plane and is subsequently deployed through a rotation around its edge BC. As shown in Fig. 1b, this deployment results in the displacement w_A of vertex A along the z direction and a volume V_{ABC} under the triangle

$$V_{ABC} = \frac{w_{A}||AB||^{2}}{6} \frac{\sin \alpha}{\sin(\alpha + \beta)} \sqrt{\sin^{2}\beta - \frac{w_{A}^{2}}{||AB||^{2}}},$$
 (1)

where ||AB|| indicates the length of AB. By focusing on the x-y plane, through simple geometrical considerations, one can see that if $\beta \in [\pi/4 - \alpha/2, \pi/2 - \alpha]$, the projection of vertex A during the deployment intersects the circle circumscribed to the initial configuration (Fig. 1b) for a displacement w_A^c defined as

$$w_{\rm A}^{\rm c} = ||{\rm AB}|| \sqrt{1 - \frac{\cos^2 \beta}{\sin^2(\alpha + \beta)}}$$
 (2)

It follows from the inscribed angle theorem⁴⁵ that for $w_A = w_A^c$, the angle α is recovered on the x-y plane (see Supplementary Information section 1 for details). As such, if triangles of this type are used as building blocks to form origami polyhedra, the assembled systems will have two distinct compatible configurations: one flat (identified by $w_A = 0$) and one expanded (identified by $w_A = w_A^c$). By contrast, any configuration

^{1.} A. Paulson School of Engineering and Applied Sciences, Harvard University, Cambridge, MA, USA. 2Department of Building Structures and Geotechnical Engineering, University of Seville, Seville, Spain, 3Wyss Institute for Biologically Inspired Engineering Harvard University, Cambridge, MA, USA, 4Hoberman Associates, New York, NY, USA, 5Graduate School of Design, Cambridge, MA, USA. 6 Kavli Institute, Harvard University, Cambridge, MA, USA. 7 These authors contributed equally: David Melancon, Benjamin Gorissen. e-mail: choberman@gsd.harvard.edu; bertoldi@seas.harvard.edu

Article

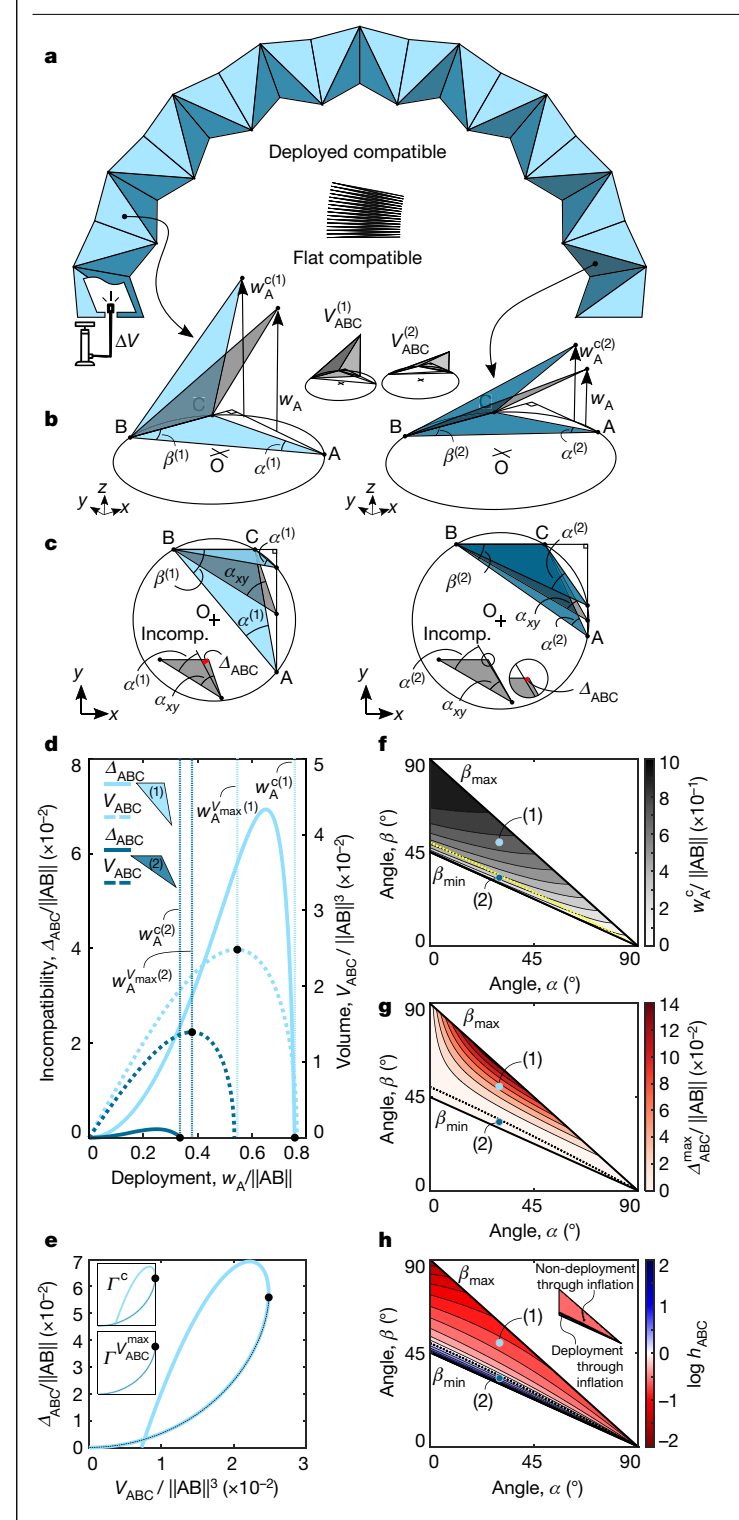


Fig. 1| **Triangular facets as building blocks for large-scale inflatable and bistable origami structures. a**, Schematics illustrating the deployment via inflation of a large-scale origami structure comprising triangular facets. **b**, Deployment of two triangular building blocks ABC with angles $(\alpha^{(1)}, \beta^{(1)})$ and $(\alpha^{(2)}, \beta^{(2)})$. **c**, Projected view of the deployment showing the two intersection points with the circle centred in O. **d**, Evolution of incompatibility, $\Delta_{\rm ABC}$, and underlying volume, $V_{\rm ABC}$, as a function of the deployment height, $w_{\rm A}$. **e**, Evolution of incompatibility, $\Delta_{\rm ABC}$, as a function of the underlying volume, $V_{\rm ABC}$. **f-h**, Contour maps of the compatible deployment height, $w_{\rm A}^{\rm C}({\bf f})$, maximum incompatibility, $\Delta_{\rm ABC}^{\rm max}({\bf g})$ and inflation constraint, $h_{\rm ABC}({\bf h})$.

with $0 < w_A < w_A^c$ will be geometrically frustrated, with incompatibility, Δ_{ABC} , that can be estimated as

$$\Delta_{ABC} = ||AC_{xy}|| \sin(\alpha_{xy} - \alpha), \tag{3}$$

where AC_{xy} and α_{xy} are the projection on the x-y plane of edge AC and angle α , respectively (note that $\alpha_{xy} = \alpha$ only for $w_A = 0$ and w_A^c ; see the inset in Fig. 1c).

Therefore, to accommodate geometric frustration and realize closed origami shapes (that is, shapes forming a closed inflatable cavity) capable of switching between two compatible configurations, we connect stiff triangular building blocks to stretchable hinges. Importantly, whereas polyhedra composed of rigid triangular faces connected by perfect rotational hinges are known to be either rigid for volume invariant during deployment whereas to be bistable. Indeed, for hinges with stiff facets and flexible hinges to be bistable. Indeed, for hinges with low enough bending stiffness, we expect the energy profile of the closed origami to show two local minima corresponding to the flat and expanded compatible states (where the energy in the system can only be attributed to hinge bending), separated by an energy barrier caused by the deformation of the facets and the hinges required to accommodate geometric incompatibility.

To gain more insights into the behaviour of our building blocks, we focus on the deployment of two triangles with $(\alpha^{(1)}, \beta^{(1)}) = (30^{\circ}, 50^{\circ})$ and $(\alpha^{(2)}, \beta^{(2)}) = (30^{\circ}, 33^{\circ})$. In Fig. 1d, we report the evolution of the incompatibility, Δ_{ABC} , and the underlying volume, V_{ABC} , as a function of the deployment height, w_A , for both triangles. We find that the triangle with $\beta^{(1)} = 50^{\circ}$ is characterized by both larger w_A^c and maximum incompatibility, $\Delta_{ABC}^{max} = max(\Delta_{ABC})$. However, for this triangle, the expanded compatible state is located after the configuration corresponding to the maximum underlying volume ($w_A^{c(1)} > w_A^{V_{ABC}^{max}(1)}$) and, therefore, cannot be reached when $V_{\rm ABC}$ is controlled. As such, whereas we expect a closed origami structure realized using these triangles to have two stable states with very different internal volume, we cannot use inflation to switch between the two of them. By contrast, the triangle with $\beta^{(2)} = 33^{\circ}$ exhibits much smaller $\Delta_{\rm ABC}^{\rm max}$ and $w_{\rm A}^{\rm c}$, but can be deployed when controlling the volume as $w_{\rm A}^{\rm c(2)} < w_{\rm A}^{V_{\rm ABC}^{\rm max}(2)}$. This suggests that closed origami realized using this triangle can be deployed using inflation, but have an expanded configuration very similar to the flat one. Further, we expect such structures to be only marginally bistable, as small perturbations are enough to overcome the energy barrier associated with the small $\Delta_{ABC}^{max(2)}$.

Whereas in Fig. 1b–d we focus on two geometries, we next consider all deployable triangles (that is, triangles with $\pi/4 - \alpha/2 \le \beta \le \pi/2 - \alpha$) and look for those that can potentially lead to deployable structures that are simultaneously bistable and inflatable. Towards this end, we use w_A^c to estimate the change in shape between the compatible states and Δ_{ABC}^{max} to evaluate bistability (that is, to estimate the energy required to snap back from the expanded to the flat state). Furthermore, we introduce an inflation constraint

$$h_{\rm ABC} = \frac{\Gamma^{V_{\rm ABC}^{\rm max}}}{\Gamma^{\rm c}},\tag{4}$$

where $\Gamma^{V_{\rm ABC}^{\rm ABC}}$ and $\Gamma^{\rm c}$ are the arc lengths measured on the $\Delta_{\rm ABC}$ – $V_{\rm ABC}$ curve between the flat stable state and the state of maximum volume and between the flat and expanded stable configurations, respectively (Fig. 1e). It follows from equation (4) that only geometries with $\log h_{\rm ABC} \ge 0$ can be deployed through fluidic actuation as those are the only ones for which the expanded compatible configuration is reached before the one with maximum volume during inflation (note that $\log h_{\rm ABC} = -1.46$ and $\log h_{\rm ABC} = 0.322$ for the two triangles considered in Fig. 1b, c).

In Fig. 1f-h, we report $w_{\rm A}^{\rm c}$, $\Delta_{\rm ABC}^{\rm max}$ and $h_{\rm ABC}$ for all deployable triangles. We find that both $w_{\rm A}^{\rm c}$ and $\Delta_{\rm ABC}^{\rm max}$ are maximized in the region close

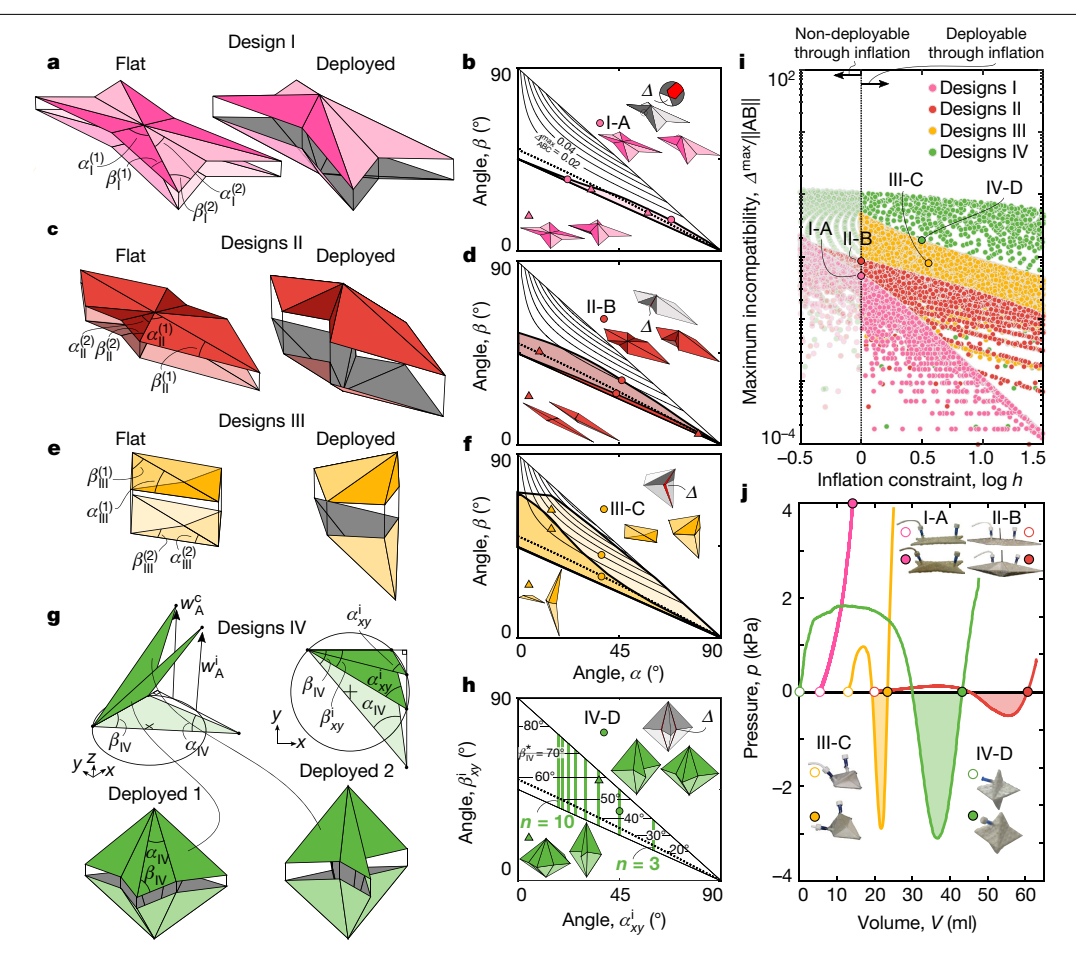


Fig. 2 | Bistable and inflatable origami shapes. a-f, Examples of Designs I (a, b), Designs II (\mathbf{c}, \mathbf{d}) and Designs III (\mathbf{e}, \mathbf{f}) geometries in both the flat and deployed stable configurations (**a**, **c**, **e**) along with the regions in the α - β space leading to inflatable structures (b, d, f). The bright and dark shaded regions in the plots represent the triangles with angles $(\alpha^{(1)}, \beta^{(1)})$ and $(\alpha^{(2)}, \beta^{(2)})$, respectively. The contour lines represent the maximum incompatibility of the triangular building blocks, Δ_{ABC}^{max} , the dashed line separates the region with positive and negative $h_{\rm ABC}$. The solid circles and triangles indicate the triangular building

blocks used to make the designs shown in the insets. g, Deployment of a triangular building block that has been initially rotated around its edge BC to have a height w_A^i . **h**, Contour map of angle β_{vv}^* required to obtain Designs IV that are both inflatable and bistable. i, Maximum incompatibility, Δ^{max} , versus the inflation constraint, h, for 500,000 random geometries of Designs I-IV. j, Pressure-volume curves recorded when testing our centimetre-scale $prototypes. See \, Supplementary \, Information \, for \, the \, rationale \, behind \, geometry \, and \, rationale \, geometry \, and \, ra$ and material selection.

to the upper boundary of the domain (that is, when $\beta \rightarrow \pi/2 - \alpha$). By contrast, the triangles deployable through inflation (for which $\log h_{ABC} \ge 0$) are all close to the lower boundary of the domain (that is, when $\beta \rightarrow \pi/4 - \alpha/2$) and show small values of W_A^c and Δ_{ABC}^{max} As such, these results indicate that we cannot realize closed origami structures that are at the same time bistable and inflatable using a single triangle building block.

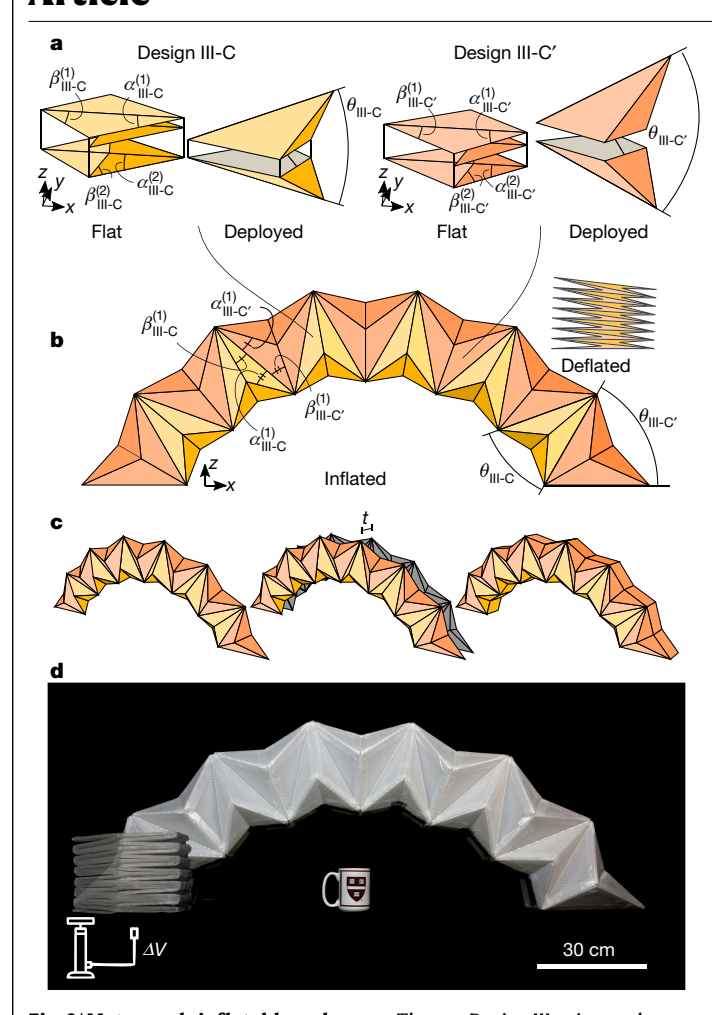
Extending the design space to enable deployment via inflation

In an attempt to realize inflatable closed origami structures with stable flat and expanded configurations, we turn our focus to systems realized by assembling two different triangles with internal angles $(\alpha^{(1)}, \beta^{(1)})$ and $(\alpha^{(2)}, \beta^{(2)})$. To begin with, we arrange 2n triangles of each type to form two identical layers with n-fold symmetry and connect them at their outer boundaries (Fig. 2a, c). The resulting star-like structures (reminiscent of an origami waterbomb base^{38,49}) define an internal volume $V = 2n(V_{ABC}^{(1)} + V_{ABC}^{(2)})$, exhibit geometric incompatibility $\Delta = 2n(\Delta_{ABC}^{(1)} + \Delta_{ABC}^{(2)})$ and are inflatable only if $\log h = \log(\Gamma^{V_{ABC}}) > 0$, where $\Gamma^{V_{ABC}}$ and Γ^{c} are the arc lengths measured on the $\Delta - V$ curve between the states with V = 0 and $V = V^{max} = max(V)$ and between the two stable configurations, respectively. However, it is important to note that to realize these star-like structures, the pair of triangles

cannot be arbitrarily chosen. This is because geometric compatibility is guaranteed only if the two triangles have (1) identical deployed compatible height (that is, $w_A^{c(1)} = w_A^{c(2)}$), (2) connecting deployed edges (either AB or AC) of equal length, and (3) angles that satisfy $\alpha^{(1)} + \alpha^{(2)} = \pi/n$.

As shown in Fig. 2a, we first connect the two triangles via their longest edge ($||AB^{(1)}|| = ||AB^{(2)}||$) and refer to these structures as Designs I. We identify all possible geometries by enforcing requirements 1-3 and find that designs deployable through inflation (for which $\log h \ge 0$) not only have a deployed shape almost indistinguishable from the initial flat one (see insets of structures in Fig. 2b) but also are made of two triangles with very low Δ_{ABC}^{max} (see area highlighted in magenta in Fig. 2b). As such, the inflatable Designs I exhibit very low maximum incompatibility $\Delta^{max} = max(\Delta)$ (see magenta markers in Fig. 2i for 500,000 randomly chosen geometries). To investigate the performance of these inflatable designs, we fabricate and test the geometry with $\log h \ge 0$ and the highest Δ^{max} (Design I-A with $(\alpha_{I-A}^{(1)},\beta_{I-A}^{(1)})$ = $(22^{\circ},35^{\circ})$ and $(\alpha_{I-A}^{(2)},\beta_{I-A}^{(2)})$ = $(68^{\circ},14^{\circ})$ for which $\Delta^{max}/||AB||$ = 2.67×10^{-2} ; see magenta circular marker in Fig. 2i). A centimetre-scale prototype with $||AB^{(1)}|| = ||AB^{(2)}|| = 60$ mm is constructed by connecting threedimensional-printed stiff triangular facets with compliant hinges made of thin polyester sheets and an inflatable cavity is formed by coating it with a 0.5-mm-thick layer of silicone rubber (see insets in Fig. 2j, Supplementary Information section 2, Supplementary Video 1 for details).

Article



 $\label{lem:construction} \textbf{Fig. 3} | \textbf{Metre-scale inflatable archway. a}, \textbf{The two Design III units used to} \\ \textbf{construct the arch. b}, \textbf{Schematics illustrating an inflatable archway comprising} \\ \textbf{six Design III-C} \\ \textbf{and seven Design III-C' units. c}, \textbf{To facilitate inflation}, \textbf{we create} \\ \textbf{a single cavity by cutting all units through their } \textbf{x-z} \\ \textbf{mirror plane}, \textbf{separating the} \\ \textbf{two resulting parts by a distance} \\ \textbf{t}, \textbf{and connecting them with rectangular} \\ \textbf{facets. d}, \textbf{Fabricated metre-scale inflatable arch in its flat and deployed stable} \\ \textbf{configurations}.$

The sample is then deployed by supplying water at a constant rate of $10\,\mathrm{ml\,min^{-1}}$ with a syringe pump, while monitoring the pressure with a pressure sensor (see Supplementary Information section 3 for details). We find that the pressure, p, increases monotonically with V until the maximum volume for the cavity is reached (Fig. 2j, Supplementary Video 2). As such, our test reveals that the Δ^{max} of this design is not large enough to make the fabricated structure bistable.

Next, with the goal of increasing the geometric incompatibility of the inflatable designs, we investigate the response of star-like structures in which the longest edge of one triangle, AB⁽¹⁾, is connected to the shortest edge of the other one, AC⁽²⁾ (we refer to these designs as Designs II; Fig. 2c). Again, we impose requirements 1–3 to identify all possible geometries and find that those deployable through inflation comprise two very distinct triangles: a first one with low $\Delta_{\rm ABC}^{\rm max}$ but $\log h_{\rm ABC}^{(1)} > 0$ (see area highlighted in dark red in Fig. 2d) and a second one with substantially larger $\Delta_{\rm ABC}^{\rm max}$ but $\log h_{\rm ABC}^{(2)} < 0$ (see area highlighted in bright red in Fig. 2d). Remarkably, we find that the combination of these different triangles results in inflatable designs with higher maximum incompatibility compared with Designs I (see red markers in Fig. 2i for 500,000 randomly chosen geometries). As a result, when we fabricate and test the inflatable geometry that maximizes $\Delta^{\rm max}$ (Design II-B with $(\alpha_{\rm II-B}^{(1)}, \beta_{\rm II-B}^{(1)}) = (43.6^{\circ}, 25.2^{\circ})$ and $(\alpha_{\rm II-B}^{(2)}, \beta_{\rm II-B}^{(1)}) = (46.4^{\circ}, 33.5^{\circ})$ for

which $\Delta^{\text{max}}/||\text{AB}|| = 8.58 \times 10^{-2}$; see red marker in Fig. 2i), we observe a negative pressure region (see red curve in Fig. 2j, Supplementary Video 2). This confirms the presence of an expanded stable configuration that can be reached through fluidic actuation (see Supplementary Fig. 23 for details) and indicates the existence of a threshold value of $\Delta^{\text{max}}/||\text{AB}||$ (dependent on materials and fabrication process) that marks the transition from monostable to bistable behaviour.

Whereas the connection of two different triangles side by side enables us to design inflatable and bistable structures, it limits us to star-like shapes. To expand the range of shapes, we next arrange the two triangles on top of each other in the flat configuration and mirror them twice to form an inflatable cavity (we refer to these structures as Designs III; Fig. 2e). This leads to geometries comprising eight triangles that are initially flat and transform into wedge-like shapes upon deployment. As for Designs I and Designs II, geometric compatibility for Designs III requires a pair of triangles with $w_A^{c(1)} = w_A^{c(2)}$ and $||AB^{(1)}|| = ||AC^{(2)}||$, but the closure of the cavity is only possible if $\alpha_{III}^{(1)} = \alpha_{III}^{(2)}$. By imposing these constraints and $\log h \ge 0$, we find that inflatable Designs III can be realized by combining two triangles with $\log h_{ABC} < 0$ and, therefore, substantially larger Δ_{max}^{ABC} (see areas highlighted in yellow in Fig. 2f). This is because the internal volume of Designs III is defined by the difference between $V_{ABC}^{(1)}$ and $V_{ABC}^{(2)}$ (that is, $V = 4(V_{ABC}^{(1)} - V_{ABC}^{(2)})$) instead of their sum, as for Designs I and Designs II. Importantly, by plotting Δ^{\max} versus h for 500,000 randomly chosen Designs III, we find that these geometries are characterized by much larger maximum incompatibility in the inflatable domain. As a result, when we fabricate and test Design III-C with $(\alpha_{\text{III-C}}^{(1)}, \beta_{\text{III-C}}^{(1)}) = (37.1^{\circ}, 30.0^{\circ})$ and $(\alpha_{\text{III-C}}^{(2)}, \beta_{\text{III-C}}^{(2)}) = (37.1^{\circ}, 40.6^{\circ})$, (for which $\Delta^{\text{max}}/||\text{AB}|| = 9.93 \times 10^{-2})$, we record even larger values of negative pressure (that is, larger energy barrier preventing the snap back) compared with the previous bistable Design II-B (Fig. 2j, Supplementary Video 2).

So far, all identified designs (that is, Designs I–III) have been realized by assembling triangles that initially lie in the x-y plane and recover their angle α on such a plane for $w_{\rm A}=w_{\rm A}^{\rm c}$. However, the triangle in the x-y plane can also be seen as the projection of a triangle with internal angles α and β that has been initially rotated around its edge BC to have a height $w_{\rm A}^{\rm i}$ and projected angles $\alpha_{xy}^{\rm i}$ and $\beta_{xy}^{\rm i}$ (Fig. 2g). In this case, if $\beta_{xy}^{\rm i} \in [\pi/4 - \alpha_{xy}^{\rm i}/2, \pi/2 - \alpha_{xy}^{\rm i}]$ the angle $\alpha_{xy}^{\rm i}$ is preserved for two distinct deployment heights, $w_{\rm A}^{\rm i}$ and $w_{\rm A}^{\rm c}$ (see inset in Fig. 2g, Supplementary Information section 1 for details). As such, we can use these triangles as building blocks to realize star-like origami shapes with two expanded stable configurations corresponding to $w_{\rm A}^{\rm i}$ and $w_{\rm A}^{\rm c}$. An interesting feature of this family of structures (which we refer to as Designs IV) is that if we select $\alpha_{xy}^{\rm i} = \pi/n \, (n=3,4,...)$ and

$$\beta_{\text{IV}} \ge \beta_{\text{IV}}^* = \tan^{-1}(\sqrt{2} \tan \beta_{xy}^{\text{i}}), \tag{5}$$

 β_{IV}^* denoting a critical threshold value, the resulting origami are bistable and inflatable, even if made out of a single triangular building block (see Supplementary Information section 1 for details). This is because, for $\beta_{\text{IV}} \geq \beta_{\text{IV}}^*$, V_{ABC} monotonically decreases when deploying the triangle from w_{A}^i to w_{A}^c , so the compatible state corresponding to w_{A}^c can always be reached by deflation. To demonstrate the concept, in Fig. 2i, we consider 500,000 different geometries of Designs IV for which $\alpha_{xy}^i = \pi/4$, $\beta_{xy}^i \in [\pi/4 - \alpha_{\text{IV}}/2, \pi/2 - \alpha_{\text{IV}}]$ and $\beta_{\text{IV}} \in [\beta_{xy}^i, \pi/2[$, and find that all geometries with $\beta_{\text{IV}} \geq \beta_{\text{IV}}^*$ are inflatable. Furthermore, as β_{IV}^* is not affected by α_{xy}^i (see map of β_{IV}^* in Fig. 2h), an inflatable origami structure can be realized by assembling highly incompatible triangles lying near the upper bound of their design space. This results in inflatable designs with a maximum incompatibility, Δ^{max} , much higher than Designs I-III and with a flat stable state in the x-z-plane (as for β = $\pi/2 - \alpha$ the compatible deployment height is such that the deployed triangle lies in the orthogonal x-z-z-plane with w_{A}^c =||AC||; see Supplementary Information section 1 for details). In full agreement with these findings, when we fabricate and test Design IV-D with ($\alpha_{\text{IV-D}}$, $\beta_{\text{IV-D}}$) = (29°, 56°) and

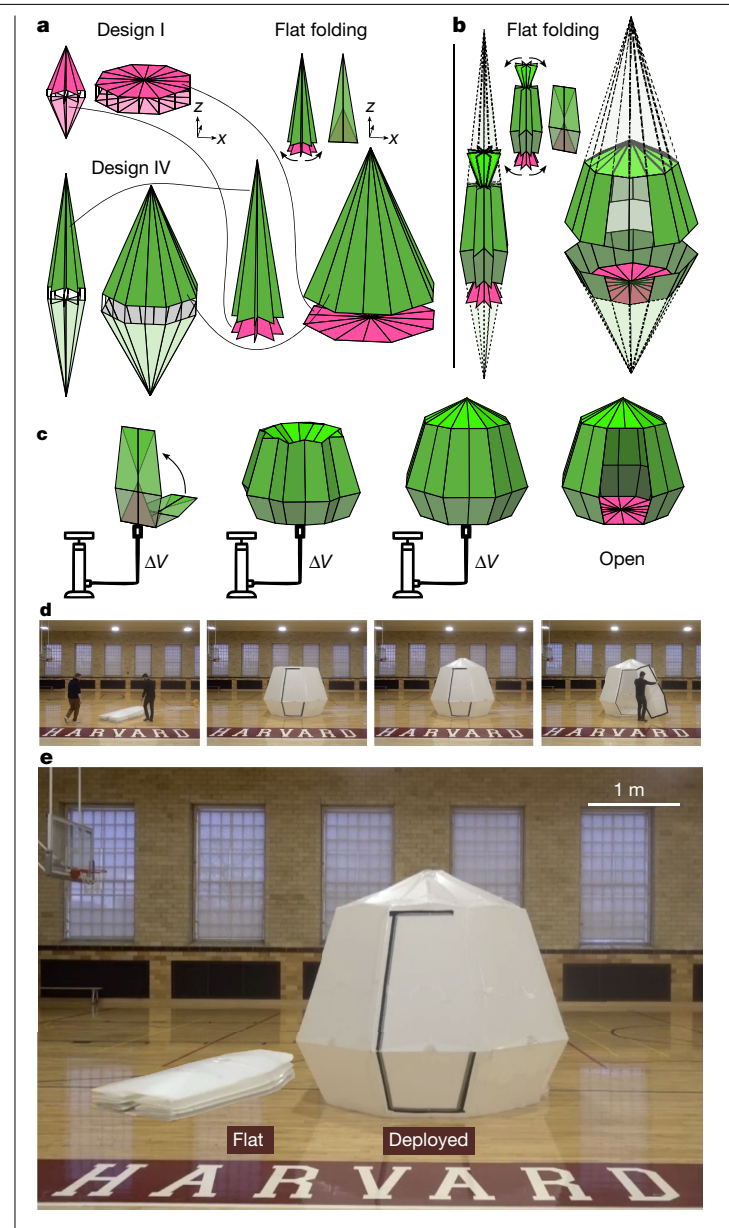


Fig. 4 | Metre-scale inflatable shelter. a, A tent-like design can be created by merging one layer of a Design I with another one of a Design IV. Note in that the initial, zero-volume configuration of the tent, both layers are in their compatible expanded state, whereas in the final inflated configuration of the tent, both layers are in their initial state (flat for Design I and initially rotated for Design IV). b, The initial volume can be further decreased by truncating the triangular facets into quadrilaterals and arranging successive layers of Design IV. c, Schematics illustrating the deployment process. d, The fabricated metre-scale inflatable shelter can be inflated from a compact state to a fully deployed state. Owing to multistability, the door can be opened, making the internal space accessible. e, Flat-folded and deployed state of the metre-scale inflatable shelter.

 $(\alpha_{xy}^i, \beta_{xy}^i) = (45^\circ, 33^\circ)$ (for which $\Delta^{max}/||AB|| = 2.05 \times 10^{-1}$), we record the largest negative pressure and energy barrier in the deployed stable state (see green curve in Fig. 2j, Supplementary Video 2).

Metre-scale functional structures

As a next step, we use the simple geometries presented in Fig. 2 as a basis to design functional and easily deployable structures for real-world applications and build them at the metre scale.

First, we use the expanded wedge-like shapes of Designs III as building blocks to realize an inflatable archway. Focusing on Design III-C. we find that in the expanded stable state it has an opening angle $\theta_{\text{III-C}} = 40^{\circ}$ (Fig. 3a). To design a deployable arch, we couple this unit with a different geometry of the same design family (which we referred to as Design III-C') that (1) is bistable and deployable through inflation, (2) has an edge AB of equal length, (3) has an opening angle $\theta_{\text{III-C}}$ such that when we alternate m+1 units of Design III-C' with m units of Design III-C, we span an angle of 180° in the expanded configuration, and (4) has the larger triangle (referred to as triangle 1 in Fig. 2) identical to that of Design III-C but mirrored (that is, $\alpha_{\text{III-C}}^{(1)} = \beta_{\text{III-C}}^{(1)}$ and $\beta_{\text{III-C}}^{(1)} = \alpha_{\text{III-C}}^{(1)}$; Fig. 3b) to ensure compactness in the flat state. By inspecting the database of Fig. 2j, we find that for m = 6, all above requirements are satisfied when Design III-C' is characterized by $(\alpha_{\text{III-C}}^{(1)}, \beta_{\text{III-C}}^{(1)}, \alpha_{\text{III-C}}^{(2)}, \beta_{\text{III-C}}^{(2)}) = (30^\circ, 37^\circ, 30^\circ, 51^\circ)$. However, as the resulting archway comprises 13 inflatable cavities, multiple pressure inputs would be needed to inflate it. To simplify the deployment process, we modify the structure by cutting it through the x-z mirror plane, separating the two resulting parts by a distance t, and connecting them with rectangular facets (see insets in Fig. 3c). As this procedure does not affect the geometric deployment of the triangles, we expect the additional facets to have a negligible impact on the structure's multistability, but to facilitate its inflatability by creating a single cavity. In Fig. 3d, we show a metre-scale version of this archway with ||AB|| = 30 cm and t = 10 cm constructed out of corrugated plastic sheets (clear 8 ft × 4 ft, 4-mm-thick sheets). To build this structure, we use a digital cutting system to cut two parts (each comprising both triangular building blocks and rectangular facets; Supplementary Fig. 20) and pattern the hinges by scoring the sheets to locally reduce the thickness of the material. We then connect the two digitally cut parts using adhesive tape to form an airtight cavity (see Supplementary Information section 2 for details). In the folded configuration, the structure has a height of 20 cm and a width of 30 cm. Upon pressurization, it inflates into a 60-cm-tall and 150-cm-wide archway that, because of its multistability, preserves its shape even when the pressure is suddenly released (Supplementary Video 3). Finally, it can be folded back to the initial flat state by applying vacuum to overcome the energy barrier (Supplementary Video 3).

Another strategy to realize functional shapes is to merge components of different design families together to form a single cavity. As an example, we can create an inflatable tent-like geometry by combining one layer of a Design I with another one of a Design IV (Fig. 4a). To ensure successful merging, the two layers must have (1) outer edges BC of equal length, and (2) the same x-y projection in the two compatible states (that is, $\alpha_1^{(1)} = \alpha_1^{(2)} = \alpha_{xy}^i$ and $\beta_1^{(1)} = \beta_1^{(2)} = \beta_{xy}^i$). Furthermore, to realize structures with a fully flat compatible state, we choose the triangles to lie on the upper boundary of the deployable domain (that is, triangles with $\beta_1^{(1)} = \pi/2 - \alpha_1^{(1)}$ and $\beta_2^{(2)} = \pi/2 - \alpha_1^{(2)}$. By imposing these constraints, we can design tent-like structures that can be folded flat and expanded via inflation (see Supplementary Fig. 24 for a centimetre-scale version), but their compactness is limited by the long AB edge of the Design IV. To further decrease the occupied volume in the compact state, we truncate the triangular building blocks of the Design IV layer into quadrilaterals and add additional layers of Design IV, some of which can be folded inwardly. As shown in Fig. 4b, these operations not only reduce the initial volume but also result in a more liveable sheltered space in the deployed state. To demonstrate this strategy, we fabricate the structure shown in Fig. 4b at the metre scale, applying the same construction process used for the inflatable archway (see Supplementary Information section 2, Supplementary Video 4 for details). As shown in Fig. 4c, d, the structure can be folded completely flat (with the ceiling folded inward) to occupy a space of $1.0 \times 2.0 \times 0.25$ m. When an input pressure is provided, the structure first expands to a stable configuration with the roof folded inward. Upon further pressurization, the roof snaps outwards and the final deployed shape of $2.5 \times 2.6 \times 2.6$ m is reached. Importantly, because of the multistability, at this point the

Article

door can be opened without impacting structural integrity, making the internal space accessible. Finally, using a vacuum, the shelter can be folded back to the flat configuration (Supplementary Video 3).

Conclusion

In summary, we have demonstrated how geometry can be efficiently exploited to realize pressure-deployable origami structures characterized by two stable configurations—one compact and one expanded. The design methodology presented in this work could be extended both to larger and smaller scales if properly accounting for loading conditions and fabrication challenges^{4,10,11,20}. As our functional structures are multistable, they can also be designed to achieve target deployment sequences (Supplementary Fig. 25). In addition, by introducing building blocks comprising more than two different facets, we expect to further expand the range of achievable shapes (Supplementary Fig. 26). To that end, complementary to our geometric model and experiments, a mechanical model capable of predicting the full energy landscape^{39,50} could provide a useful tool to guide such exploration. Finally, building on our results, deployable structures able to switch between targeted stable states could be efficiently identified by generalizing our design rules to arbitrary origami polyhedra and, combining them with stochastic optimization algorithms, solve the inverse design problem.

Online content

Any methods, additional references, Nature Research reporting summaries, source data, extended data, supplementary information, acknowledgements, peer review information; details of author contributions and competing interests; and statements of data and code availability are available at https://doi.org/10.1038/s41586-021-03407-4.

- 1. Pellegrino, S. Deployable Structures in Engineering (Springer-Verlag, 2014).
- 2. You, Z. & Pellegrino, S. Foldable bar structures. Int. J. Solids Struct. 34, 1825-1847 (1997).
- Liu, Y., Du, H., Liu, L. & Leng, J. Shape memory polymers and their composites in aerospace applications: a review. Smart Mater. Struct. 23, 023001 (2014).
- Puig, L., Barton, A. & Rando, N. A review on large deployable structures for astrophysics missions. Acta Astron. 67, 12–26 (2010).
- Zhao, J.-S., Chu, F. & Feng, Z.-J. The mechanism theory and application of deployable structures based on SLE. Mech. Mach. Theory, 44, 324–335 (2009).
- Mira, L. A., Thrall, A. P. & De Temmerman, N. Deployable scissor arch for transitional shelters. Autom. Constr. 43, 123–131 (2014).
- Thrall, A. P., Adriaenssens, S., Paya-Zaforteza, I. & Zoli, T. P. Linkage-based movable bridges: design methodology and three novel forms. Eng. Struct. 37, 214–223 (2012).
- Arnouts, L. I. W., Massart, T. J., De Temmerman, N. & Berke, P. Structural optimisation of a bistable deployable scissor module. In Proc. IASS Annual Symposium 2019—Structural Membranes 2019 (eds Lázaro, C. et al.) (2019).
- García-Mora, C. J. & Sánchez-Sánchez, J. Geometric method to design bistable and non bistable deployable structures of straight scissors based on the convergence surface. Mech. Mach. Theory 146, 103720 (2020).
- Cadogan, D., Stein, J. & Grahne, M. Inflatable composite habitat structures for lunar and Mars exploration. Acta Astron. 44, 399–406 (1999).
- Block, J., Straubel, M. & Wiedemann, M. Ultralight deployable booms for solar sails and other large gossamer structures in space. Acta Astron. 68, 984-992 (2011).
- Sifert, E., Reyssat, E., Bico, J. & Roman, B. Programming stiff inflatable shells from planar patterned fabrics. Soft Matter 16, 7898–7903 (2020).
- Siéfert, E., Reyssat, E., Bico, J. & Roman, B. Bio-inspired pneumatic shape-morphing elastomers. Nat. Mater. 18, 16692–16696 (2019).
- 14. Usevitch, N. S. et al. An untethered isoperimetric soft robot. Sci. Robot. 5, eaaz0492 (2020).
- 15. Skouras, M. et al. Designing inflatable structures. ACM Trans. Graph. **33**, 63 (2014).
- Rus, D. & Tolley, M. T. Design, fabrication and control of origami robots. Nat. Rev. Mater. 3, 101–112 (2018).
- Onal, C. D., Wood, R. J. & Rus, D. An origami-inspired approach to worm robots. IEEE ASME Trans. Mechatron. 18, 430–438 (2013).

- Onal, C. D., Tolley, M. T., Wood, R. J. & Rus, D. Origami-inspired printed robots. IEEE ASME Trans. Mechatron. 20, 2214–2221 (2015).
- Li, S. et al. A vacuum-driven origami "magic-ball" soft gripper. In 2019 International Conference on Robotics and Automation (ICRA) 7401–7408 (IEEE, 2019).
- Miskin, M. Z. et al. Graphene-based bimorphs for micron-sized, autonomous origami machines. Proc. Natl Acad. Sci. USA 115, 466-470 (2018).
- Silverberg, J. L. et al. Using origami design principles to fold reprogrammable mechanical metamaterials. Science 345, 647–650 (2014).
- Dudte, L. H., Vouga, E., Tachi, T. & Mahadevan, L. Programming curvature using origami tessellations. Nat. Mater. 15, 583–588 (2016).
- Filipov, E. T., Tachi, T. & Paulino, G. H. Origami tubes assembled into stiff, yet reconfigurable structures and metamaterials. Proc. Natl Acad. Sci. USA 112, 12321–12326 (2015).
- Overvelde, J. T. B., Weaver, J. C., Hoberman, C. & Bertoldi, K. Rational design of reconfigurable prismatic architected materials. *Nature* 541, 347–352 (2017).
- Iniguez-Rabago, A., Li, Y. & Overvelde, J. T. B. Exploring multistability in prismatic metamaterials through local actuation. Nat. Commun. 10, 5577 (2019).
- Seymour, K. et al. Origami-based deployable ballistic barrier. In Proc. 7th International Meeting on Origami in Science Mathematics and Education 763–778 (2018).
- Del Grosso, A. & Basso, P. Adaptive building skin structures. Smart Mater. Struct. 19, 124011 (2010).
- 28. Tachi, T. in Origami 5 (eds Wang-Iverson, P. et al.) Ch. 20 (CRC Press, 2011).
- Zirbel, S. A. et al. Accommodating thickness in origami-based deployable arrays. J. Mech. Des. 135, 111005 (2013).
- You, Z. & Cole, N. Self-locking bi-stable deployable booms. In 47th AIAA/ASME/ASCE/ AHS/ASC Structures, Structural Dynamics, and Materials Conference AIAA 2006-1685 (ARC, 2006); https://arc.aiaa.org/doi/abs/10.2514/6.2006-1685.
- Lang., R. J. A computational algorithm for origami design. In Proc. 12th Annual ACM Symposium on Computational Geometry 98–105 (1996); https://ci.nii.ac.jp/naid/ 80009084712/en/.
- Demaine, E. D. & Mitchell, J. S. B. Reaching folded states of a rectangular piece of paper. In Proc. 13th Canadian Conference on Computational Geometry (CCCG 2001) 73–75 (2001).
- Demaine, E. D. & Tachi, T. Origamizer: a practical algorithm for folding any polyhedron. In Proc. 33rd International Symposium on Computational Geometry (SoCG 2017) 34:1–34:15 (2017).
- Martinez, R. V., Fish, C. R., Chen, X. & Whitesides, G. M. Elastomeric origami: programmable paper-elastomer composites as pneumatic actuators. Adv. Funct. Mater. 22, 1376–1384 (2012).
- Li, S., Vogt, D. M., Rus, D. & Wood, R. J. Fluid-driven origami-inspired artificial muscles. Proc. Natl Acad. Sci. USA 114, 13132–13137 (2017).
- Kim, W. et al. Bioinspired dual-morphing stretchable origami. Sci. Robot. 4, eaay3493
 (2019).
- Kamrava, S., Mousanezhad, D., Ebrahimi, H., Ghosh, R. & Vaziri, A. Origami-based cellular metamaterial with auxetic, bistable, and self-locking properties. Sci. Rep. 7, 46046 (2017).
- Hanna, B., Lund, J., Lang, R., Magleby, S. & Howell, L. Waterbomb base: a symmetric single-vertex bistable origami mechanism. Smart Mater. Struct. 23, 094009 (2014).
- Cai, J., Deng, X., Ya, Z., Jian, F. & Tu, Y. Bistable behavior of the cylindrical origami structure with Kresling pattern. J. Mech. Des. 137, 061406 (2015).
- Silverberg, J. L. et al. Origami structures with a critical transition to bistability arising from hidden degrees of freedom. Nat. Mater. 14, 389–393 (2015).
- Waitukaitis, S., Menaut, R., Gin-ge Chen, B. & van Hecke, M. Origami multistability: from single vertices to metasheets. *Phys. Rev. Lett.* 114, 055503 (2015).
- Yasuda, H. & Yang, J. Reentrant origami-based metamaterials with negative Poisson's ratio and bistability. Phys. Rev. Lett. 114, 185502 (2015).
- Reid, A., Lechenault, F., Rica, S. & Adda-Bedia, M. Geometry and design of origami bellows with tunable response. *Phys. Rev. E* 95, 013002 (2017).
- Faber, J. A., Arrieta, A. F. & Studart, A. R. Bioinspired spring origami. Science 359, 1386–1391 (2018).
- 45. Dolciani, M. P., Donnelly, A. J. & Jurgensen, R. C. Modern Geometry, Structure and Method (Houghton Mifflin, 1963).
- 46. Connelly, R. The rigidity of polyhedral surfaces. *Math. Mag.* **52**, 275–283 (1979).
- Connelly, R., Sabitov, I. & Walz, A. The bellows conjecture. Contrib. Algebr. Geom. 38, 1–10 (1997).
- 48. Mackenzie, D. Polyhedra can bend but not breathe. Science **279**, 1637–1637 (1998).
- Chen, Y., Feng, H., Ma, J., Peng, R. & You, Z. Symmetric waterbomb origami. Proc. R. Soc. A 472, 20150846 (2016).
- Paulino, G. H. & Liu. K. Nonlinear mechanics of non-rigid origami: an efficient computational approach. Proc. R. Soc. A 473, 20170348 (2017).

Publisher's note Springer Nature remains neutral with regard to jurisdictional claims in published maps and institutional affiliations.

© The Author(s), under exclusive licence to Springer Nature Limited 2021

Methods

The details of the design, materials and fabrication methods are summarized in Supplementary Information sections 1, 2. The experimental procedure of the inflation with water to measure the pressure–volume curve is described in Supplementary Information section 3. Finally, additional information about extending our methodology to more complex designs is provided in Supplementary Information section 4.

Data availability

The datasets generated or analysed during the current study are available from the corresponding author on reasonable request.

Code availability

The code generated during the current study is available from the corresponding author on reasonable request.

Acknowledgements We thank E. Demaine, J. Ku, T. Tachi and Yunfang Yang for insightful discussions; S. Lindner-Liaw, M. Bhattacharya and M. Starkey for assistance in the fabrication of the centimetre-scale and large-scale structures; and A. E. Forte for his valuable comments and suggestions on the manuscript. This research was supported by NSF through the Harvard University Materials Research Science and Engineering Center grant number DMR-1420570 and DMREF grant number DMR-1922321, as well as the Fund for Scientific Research-Flanders (FWO).

Author contributions D.M., B.G., C.H. and K.B. proposed and developed the research idea. D.M. conducted the numerical calculations. D.M., B.G. and C.J.G.-M. designed and fabricated the centimetre-scale and metre-scale structures. D.M. performed the experiments. D.M., B.G. and K.B. wrote the paper. K.B. supervised the research.

Competing interests The authors declare no competing interests.

Additional information

Supplementary information The online version contains supplementary material available at https://doi.org/10.1038/s41586-021-03407-4.

Correspondence and requests for materials should be addressed to C.H. or K.B. Peer review information *Nature* thanks Larry Howell, Glaucio Paulino and the other, anonymous, reviewer(s) for their contribution to the peer review of this work. Peer reviewer reports are available.

Reprints and permissions information is available at http://www.nature.com/reprints.